

Wire-Type Ruthenium(II) Complexes with Terpyridine-Containing [2]Rotaxanes as Ligands: Synthesis, Characterization, and Photophysical Properties

Gregory J. E. Davidson,^[a] Stephen J. Loeb,^{*[a]} Paolo Passaniti,^[b] Serena Silvi,^[b] and Alberto Credi^{*[b]}

Abstract: [2]Rotaxanes based on the 1,2-bis(pyridinium)ethane⊂[24]crown-8 ether motif were prepared that contain a terminal terpyridine group for coordination to a transition-metal ion. These rotaxane ligands were utilized in the preparation of a series of heteroleptic [Ru(terpy)(terpy-rotaxane)]²⁺ complexes. The compounds were characterized by 1D and 2D ¹H NMR spectroscopy, X-ray crystallography, and high-resolution electrospray ionization mass spectrometry. The effect of using a rotaxane as a ligand was probed by UV/Vis/NIR absorption and emission spectroscopy of the Ru^{II} complexes. In contrast with the parent [Ru(terpy)₂]²⁺ complex, at room temperature the ex-

amined complexes exhibit a luminescence band in the near infrared region and a relatively long lived triplet metal-to-ligand charge-transfer (³MLCT) excited state, owing to the presence of strong-electron-acceptor pyridinium substituents on one of the two terpy ligands. Visible-light excitation of the Ru-based chromophore in acetonitrile at room temperature causes an electron transfer to the covalently linked 4,4'-bipyridinium unit and the quenching of the MLCT lumines-

cence. The ³MLCT excited state, however, is not quenched at all in rigid matrix at 77 K. The rotaxane structure was found to affect the absorption and luminescence properties of the complexes. In particular, when a crown ether surrounds the cationic axle, the photoinduced electron-transfer process is slowed down by a factor from 2 to 3. Such features, together with the synthetic and structural advantages offered by [Ru(terpy)₂]²⁺-type complexes compared to, for example, [Ru(bpy)₃]²⁺-type compounds, render these rotaxane-metal complexes promising candidates for the construction of photochemical molecular devices with a wire-type structure.

Keywords: crown compounds • electron transfer • luminescence • self-assembly • terpyridine

Introduction

The investigation of mechanically linked molecules as prototypical artificial molecular machines^[1,2] has resulted in the synthesis and characterization of a variety of threaded and interlocked systems.^[3–11] The use of [2]rotaxanes as linkers in metal-ligand self-assembly reactions^[12] provides a methodology for the organization of these molecular machines into

solid-state materials that we call “metal-organic rotaxane frameworks” (MORFs). The basic concept utilizes [2]pseudorotaxanes to construct fully interlocked [2]rotaxanes by coordination of a transition-metal complex. To date, we have used our 1,2-bis(4,4'-bipyridinium)ethane⊂DB24C8 (DB24C8 = dibenzo[24]crown-8 ether) motif (Figure 1) to

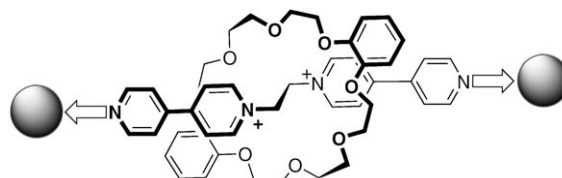


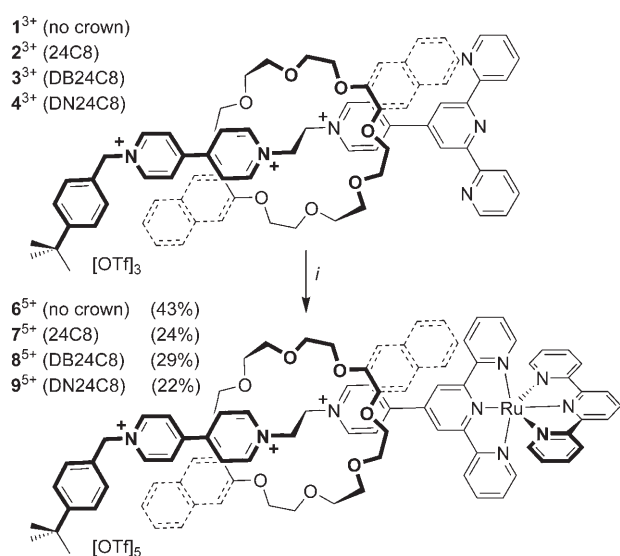
Figure 1. Utilizing transition- and lanthanide-metal-ion nodes, the [2]pseudorotaxane comprised of a 1,2-bis(4,4'-bipyridinium)ethane axle and a dibenzo[24]crown-8 ether wheel acts as a bridging ligand to form metal-organic rotaxane frameworks, MORFs.

[a] Dr. G. J. E. Davidson, Prof. S. J. Loeb
Department of Chemistry and Biochemistry
University of Windsor, Windsor, ON N9B 3P4 (Canada)
Fax: (+1)519-973-7098
E-mail: loeb@uwindsor.ca

[b] Dr. P. Passaniti, S. Silvi, Prof. A. Credi
Department of Chemistry “G. Ciamician”
University of Bologna, Bologna (Italy)
Fax: (+39)051-209-9456
E-mail: alberto.credi@unibo.it

construct a variety of interlocked molecules and materials by means of this self-assembly strategy.^[13–17] Almost any metal complex with a single, open coordination site is bulky enough to be used as an effective stopper and single metal-ion nodes result in 1D, 2D, or 3D metal–ligand frameworks with rotaxane bridging ligands (MORFs).^[18]

One of the shortcomings of any self-assembly strategy for metal-ion incorporation is that formation of the metal–ligand bonds must be compatible with maintaining the weaker non-covalent interactions between axle and wheel (ion–dipole, hydrogen bonding, and π -stacking interactions). A simple modification that would stabilize the metal–ligand interactions in either molecular rotaxanes or network polyrotaxanes and can easily be implemented is replacement of the monodentate pyridine donor with a multidentate chelator. The ligand/linker would then be a permanently interlocked [2]rotaxane constructed prior to metal–ligand self-assembly. In this vein, we have recently reported the preparation and preliminary coordination chemistry with Fe^{II} of the terpyridine-based [2]rotaxane ligands **1–4**[OTf]₃ shown in Scheme 1.^[19] Since the ligand is already a [2]rotaxane, the conditions under which chelation to a metal center is conducted do not effect the integrity of the mechanical linkage.^[20]



Scheme 1. i) One equivalent of [RuCl₃(terpy)], **5** in 1:1 EtOH/H₂O at reflux for 24 h. 24C8=[24]crown-8, DB24C8=dibenzo[24]crown-8, and DN24C8=dinaphtho[24]crown-8 ether.

In this article, we report the preparation of heteroleptic Ru^{II} complexes at reflux in polar solvents with little to no decomposition of the [2]rotaxane ligands and the results of a spectroscopic and photophysical investigation. This type of approach to bridging rotaxane ligands should 1) greatly expand the synthetic conditions under which MORF assembly can be conducted, 2) allow the preparation of MORFs with increased stability, and 3) lead to the incorporation of a

wide variety of metal ions with their own particular electronic, magnetic, or photophysical properties.

Tris(bipyridine)-type complexes of Ru^{II} (prototype: [Ru(bpy)₃]²⁺, bpy=2,2'-bipyridine) have been extensively used as photosensitizers in multicomponent and supramolecular systems,^[21] because of a unique combination of chemical stability, redox properties, luminescence intensity, and excited-state lifetime.^[22] On the other hand, bis(terpyridine)-type complexes (prototype: [Ru(terpy)₂]²⁺, terpy=2,2':6',2''-terpyridine) exhibit less favorable photophysical properties (very short excited-state lifetimes),^[23] but offer synthetic and structural advantages with respect to the use of bidentate bpy-type ligands.^[24–26] Indeed, the Ru^{II} complexes presented herein allow investigation of just such a combination of structural features and photophysical properties.

Results and Discussion

Synthesis of ruthenium(II) rotaxane complexes: We recently described the synthesis and characterization of a unique class of terpyridine-stoppered [2]rotaxanes, **1–4**[OTf]₃.^[19] The reaction of these ligands with the Ru^{III} precursor [RuCl₃(terpy)] (**5**) resulted in the formation of heteroleptic complexes, as outlined in Scheme 1. The syntheses were carried out in a 1:1 EtOH/H₂O mixture and the reaction mixture refluxed for 24 h. Generally, a sacrificial reductant, such as *N*-ethylmorpholine, was used to facilitate reduction from Ru^{III} to Ru^{II} in standard terpy chemistry, but we have observed that pyridinium-based compounds, such as **1³⁺–4³⁺**, are often base sensitive. Fortunately, these conditions proved to be sufficient for the reductions in this case and as a result a reductant was excluded from the synthetic procedure. The dark red complexes could be easily isolated and purified by column chromatography over silica with MeOH/2 M NH₄Cl/MeNO₂ (3:1:1) as the eluent, followed by salt metathesis with NaOTf producing complexes **7–9**[OTf]₅. In the case of complex **6**[OTf]₅, MeCN/H₂O/satd KNO₃ (5:4:1) was used as the eluent. The yields for all complexes ranged from 22 to 43%.

¹H NMR spectroscopy of the ruthenium(II) rotaxane complexes: The ¹H NMR spectra of the ruthenium complexes **6⁵⁺–9⁵⁺** were recorded in CD₃CN as the triflate salts. The labeling scheme is shown in Figure 2. The ¹H NMR spectra for the complexes **6⁵⁺–9⁵⁺** revealed an upfield shift of the protons H_{a-d} and H_{a'-d'}, attributed to coordination of the Ru^{II} center; this shift confirmed the formation of the complexes. For example, H_a shifted from δ =8.79 ppm for the uncomplexed rotaxane **3³⁺** to δ =7.44 ppm upon coordination to a ruthenium(II) center (complex **8⁵⁺**). A detailed comparison of the chemical shifts for the previously described [2]rotaxanes **1³⁺–4³⁺** to those of the corresponding ruthenium(II) complexes **6⁵⁺–9⁵⁺** are summarized in Table 1.

As an example, the ¹H NMR spectrum for **8⁵⁺** is shown in Figure 3. An interesting feature of these spectra is the appearance of two clearly resolved sets of resonances for the

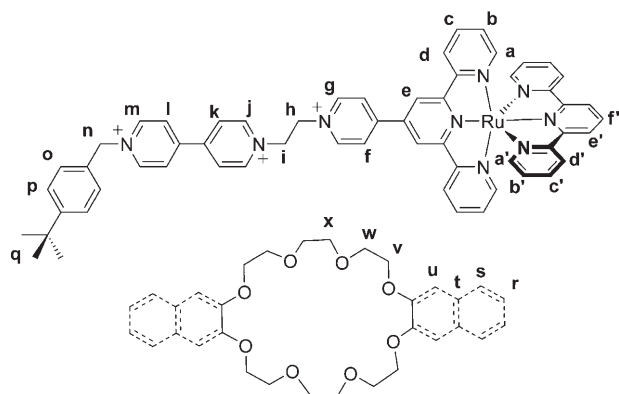


Figure 2. The basic labeling scheme used for all NMR spectral data is shown for the terpyridine based axle, the 2,2':6',2''-terpyridine and the three crown ethers used, [24]crown-8 (24C8), dibenzo[24]crown-8 (DB24C8), and dinaphtho[24]crown-8 ether (DN24C8).

different terpyridine ligands. Fortunately, proton H_f which is common to 6^{5+} – 9^{5+} and lies on the mirror plane of the complex, is unique as it integrates to half the value of the other aromatic protons. For 8^{5+} , this resonance appears as a triplet at $\delta=8.47$ ppm with a coupling constant of ~ 8 Hz. This provides a convenient starting point and allows for unambiguous assignment of all other resonances.

To distinguish between the two sets of terpy resonances, conventional 2D NMR techniques (^1H - ^1H COSY and ^1H - ^1H NOESY) were employed. Figure 4 (top) shows a ^1H - ^1H COSY spectrum for 8^{5+} in which the aforementioned H_f peak has a cross-peak with H_e along the path marked A. To jump from one ring to the other (H_e to H_d), a ^1H - ^1H NOESY (Figure 4 middle) was used. As expected, proton H_e displayed a cross-peak with the now labeled H_d along path B. Proceeding back to the ^1H - ^1H COSY, proton H_d displays three separate cross-peaks corresponding to protons

Table 1. ^1H NMR chemical shifts for [2]rotaxanes 1^{3+} – 4^{3+} and their $[\text{Ru}(\text{terpy})(\text{L})]^{2+}$ complexes 6^{5+} – 9^{5+} .

	1^{3+}	6^{5+}	$\Delta\delta$	2^{3+}	7^{5+}	$\Delta\delta$	3^{3+}	8^{5+}	$\Delta\delta$	4^{3+}	9^{5+}	$\Delta\delta$
a	8.75	7.39	-1.36	8.80	7.42	-1.38	8.79	7.44	-1.35	8.79	7.24	-1.55
b	7.52	7.21	-0.31	7.57	7.24	-0.33	7.46	7.28	-0.18	7.55	7.28	-0.27
c	8.02	7.97	-0.05	8.10	7.99	-0.11	7.98	8.05	0.07	8.05	7.99	-0.06
d	8.75	8.94	0.19	8.80	8.87	0.07	8.72	8.84	0.12	8.67	8.54	-0.13
e	8.90	9.25	0.35	8.99	9.34	0.35	8.68	8.96	0.28	8.50	8.51	0.01
f	8.55	8.75	0.20	8.52	9.08	0.56	8.23	8.74	0.51	7.54	8.59	1.05
g	8.95	9.11	0.16	9.06	9.40	0.34	9.35	9.39	0.04	9.27	9.42	0.15
h	5.27	5.38	0.11	5.45	5.53	0.08	5.68	5.70	0.02	5.68	5.75	0.07
i	5.27	5.38	0.11	5.45	5.53	0.08	5.68	5.70	0.02	5.68	5.75	0.07
j	9.03	9.11	0.08	9.37	9.40	0.03	9.41	9.39	-0.02	9.34	9.42	0.08
k	8.48	8.50	0.02	8.49	8.61	0.12	8.59	8.20	-0.39	8.37	8.23	-0.14
l	8.46	8.50	0.04	8.45	8.53	0.08	8.59	8.14	-0.45	8.08	7.70	-0.38
m	9.01	9.02	0.01	9.25	9.08	-0.17	8.98	8.98	0.00	8.50	8.70	0.20
n	5.80	5.80	0.00	5.84	5.84	0.00	5.81	5.82	0.01	5.62	5.66	0.04
o	7.45	7.45	0.00	7.45	7.49	0.04	7.46	7.49	0.03	7.54	7.51	-0.03
p	7.54	7.54	0.00	7.57	7.57	0.00	7.56	7.60	0.04	7.66	7.66	0.00
q	1.36	1.37	0.01	1.36	1.33	-0.03	1.34	1.34	0.00	1.37	1.36	-0.01
r	–	–	–	–	–	–	–	–	–	6.72	6.65	-0.07
s	–	–	–	–	–	–	–	–	–	7.22	7.43	0.21
t	–	–	–	–	–	–	6.68	6.77	0.09	–	–	–
u	–	–	–	–	–	–	6.54	6.50	-0.04	6.97	7.12	0.15

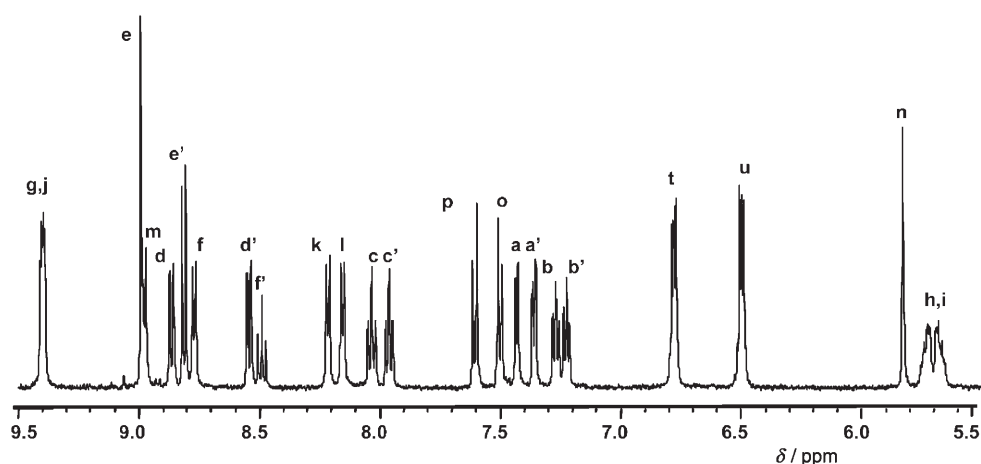


Figure 3. ^1H NMR spectrum of 8^{5+} (500 MHz, 298 K, CD_3CN); see Figure 2 for the labeling scheme.

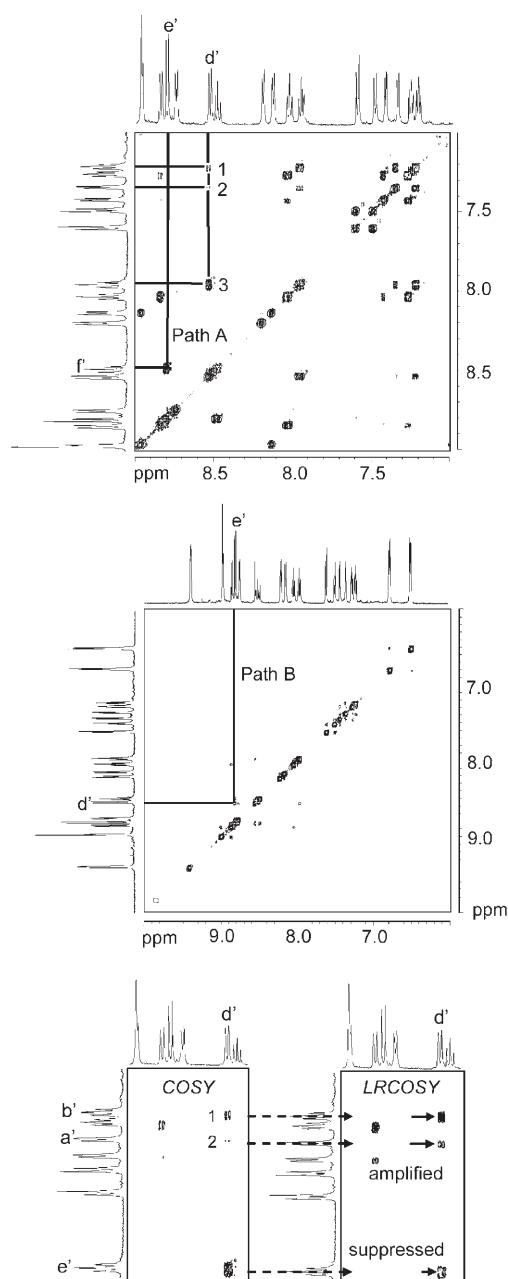


Figure 4. Top: ^1H - ^1H COSY NMR spectrum for 8^{5+} in the aromatic region. Middle: ^1H - ^1H NOESY spectrum for 8^{5+} in the aromatic region. Bottom: comparison of the ^1H - ^1H COSY (left) to the ^1H - ^1H LRCOSY (right) for complex 8^{5+} .

H_a , H_b , and H_c . Proton H_a was easily assigned based on its multiplicity. Unfortunately, assignment of protons H_b and H_c cannot be unambiguously determined in a similar manner. To assign these peaks, a ^1H - ^1H long range COSY (^1H - ^1H LRCOSY) was used which suppresses large J values (three bond coupling) and emphasizes smaller values of J (four and five bond coupling). Figure 4 (bottom) shows a close up of the ^1H - ^1H COSY and the ^1H - ^1H LRCOSY. Comparing the two spectra, a clear suppression of the peak labeled 3 can be seen, while the cross-peak intensities of the

protons marked 1 and 2 increase significantly. As a result of this suppression, peak 3 was determined to be closest to H_d (three bonds) and labeled H_c . Therefore, peak 2 corresponds to H_b . The protons of the terpyridine associated with the [2]rotaxane were assigned in a similar manner. The remaining protons of the cationic axle were assigned by using standard ^1H - ^1H COSY and ^1H - ^1H NOESY spectroscopy. The ^1H NMR spectra for Ru^{II} complexes 6^{5+} , 7^{5+} , and 9^{5+} were assigned by using an analogous approach.

X-ray structures of ruthenium(II) rotaxane complexes 8 -[OTf] $_5$ and 9 [OTf] $_5$:

Single crystals of 8 [OTf] $_5$ suitable for X-ray diffraction were grown by the diffusion of isopropyl ether into a solution of the complex and a small amount of NEt_4Cl in MeCN. Figure 5 shows a ball-and-stick representation of the cationic portion of 8 [OTf] $_5$. The [2]rotaxane axle adopts an *anti* conformation at the central $\text{NCH}_2\text{CH}_2\text{N}$ ethane unit, while the DB24C8 wheel exhibits a typical S-shaped conformation. The cationic ruthenium(II)-anchored axle interpenetrates the central cavity of the macrocycle, en-

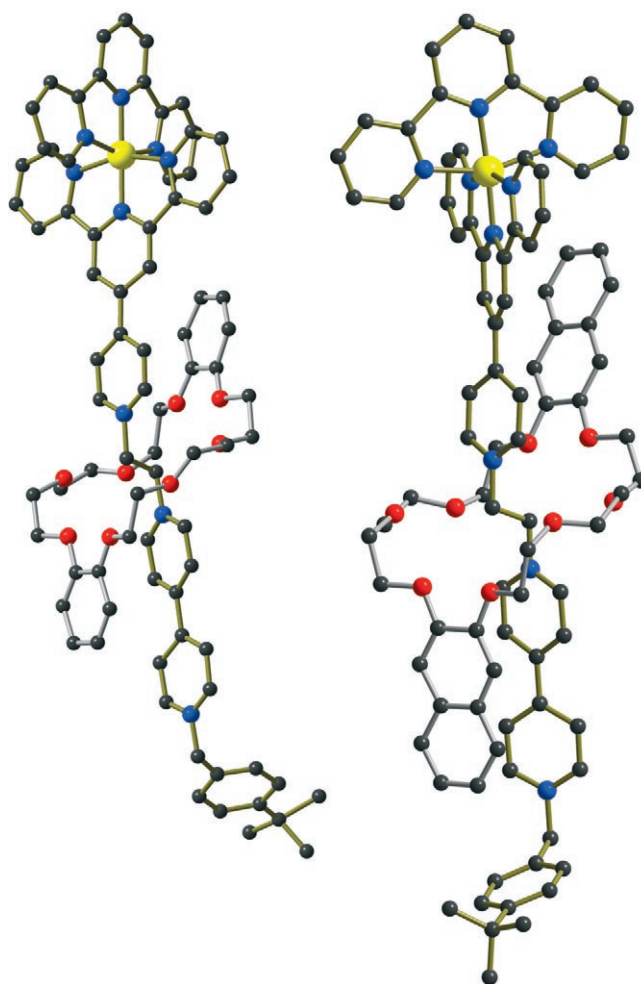


Figure 5. Ball-and-stick representations of the X-ray structures of 8 [OTf] $_5$ (left) and 9 [OTf] $_5$ (right) showing the threaded nature of the [2]rotaxanes; red = oxygen, blue = nitrogen, black = carbon, yellow = ruthenium. Anions and hydrogen atoms are omitted for clarity.

abling π -stacking interactions between the electron-rich aromatic portions of the wheel and the electron-deficient pyridinium groups of the axle.^[27] The ruthenium(II) metal center exhibits a distorted octahedral geometry as a result of the bite angle required by the terpyridine groups upon coordination.^[28] The Ru–N bond lengths and angles are similar to related Ru^{II}-bis(terpy) complexes;^[29] the Ru–N distances range from 1.957(9) to 2.080(11) Å and N–Ru–N chelating angles range from 78.5(6) to 79.8(4)°.

Single crystals of **9**[OTf]₅ were grown by the diffusion of isopropyl ether into a solution of the complex in MeNO₂; thick red plates appeared after a few days. Figure 5 shows a ball and stick representation of the cationic portion of complex **9**[OTf]₅. The structure reveals the expected *anti* conformation of the central NCH₂CH₂N portion. The ruthenium(II)-anchored cationic axle, once again, penetrates the central cavity of the wheel, and the naphthyl portions of the crown ether π -stack with the pyridinium groups of the axle. These models also reveal an edge-to-face (or T) interaction between proton H_r of the naphthyl aromatic and the aromatic ring of the *tert*-butylbenzyl capping unit as a result of the increase length of the naphtho group relative the benzo group; the H_r to Ar_{centroid} distance is 2.69 Å.

The most distinctive and important difference between the structures of **8**[OTf]₅ and **9**[OTf]₅ is the manner in which the naphthyl group of **9**[OTf]₅, which is closest to the ruthenium(II) center, is bent away from the axle; see Figure 6 (right). This occurs because the octahedral [Ru(terpy)₂]²⁺ center is sufficiently bulky to block the longer naphthyl fragment from π -stacking efficiently over both the terpy metal site and the adjacent pyridinium group, as is normally seen for these types of [2]rotaxanes and that was observed for **8**[OTf]₅, which contains the less demanding benzo group. As a result, it is necessary for the naphthyl aromatic unit to take up a position between the two terpyridine units. This can best be seen in Figure 6 (right), which shows a view down the axle in which the [Ru(terpy)₂]²⁺ unit appears as a cross in the foreground. This is achieved by having a twist in the cationic axle portion; the dihedral angle is 25.6° between

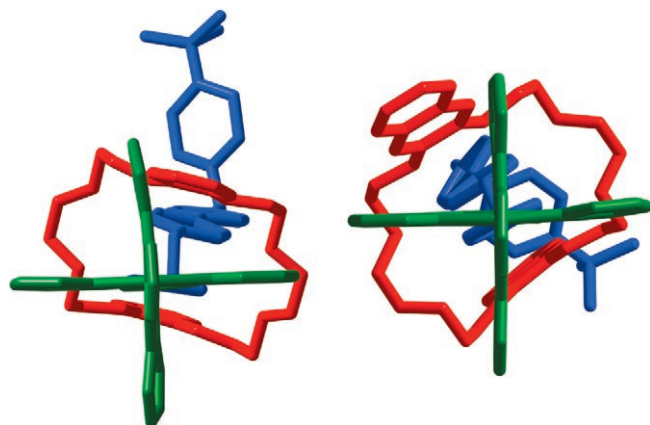


Figure 6. End-on views of the Ru^{II} rotaxane complexes **8**[OTf]₅ (left) and **9**[OTf]₅ (right) emphasizing the relative orientations of the pyridinium axle (blue), crown ether wheel (red) and ruthenium-terpy unit (green).

the pyridinium ring and the coordinated terpyridine ring, whereas in similar compounds this dihedral angle is essentially zero in order to maximize π interactions with the entire aromatic surface of the pyridinium rings. Although this twist rotates the ruthenium(II) center away from the naphtho group, the rest of the cationic portion remains unchanged and available for π -stacking. The metal center itself is unperturbed by this deformation with the Ru–N bond lengths and angles showing little variation from those found in **8**[OTf]₅ and other related compounds; the Ru–N distances range from 1.966(4) to 2.070(5) Å and N–Ru–N chelating angles range from 79.0(2) to 79.4(2)°.

Absorption and luminescence properties of the terpy-type ligands:^[30] The absorption spectra of ligands **1**³⁺ (Figure 7), **3**³⁺, and **4**³⁺ (Figure 8) in MeCN at room temperature show intense bands in the near UV region, assigned to the 4'-methylpyridinium-terpy and 4,4'-bipyridinium chromophoric units incorporated in their structures. In the case of the rotaxane ligands **3**³⁺ and **4**³⁺ the contribution from the π - π^* absorption bands of the 1,2-dioxybenzene and 1,2-dioxy-naphthalene moieties, respectively, of the interlocked crown ethers can also be observed. It is worth noting that compounds **3**³⁺ and **4**³⁺ exhibit a weak absorption tail that reaches down to 600 nm ($\epsilon \approx 500$ L mol⁻¹ cm⁻¹ at 450 nm). Such a band is assigned to charge-transfer (CT) interactions

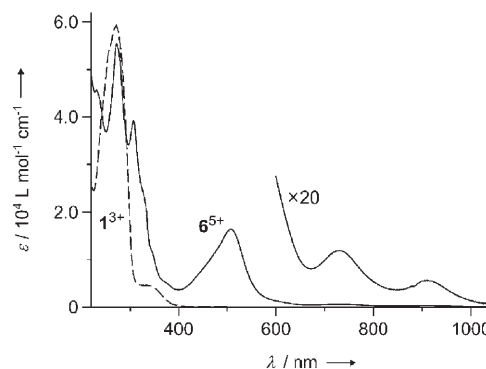


Figure 7. Absorption spectrum of the axle-like ligand **1**³⁺ (dashed line) and complex **6**⁵⁺ (full line) in MeCN solution at room temperature.

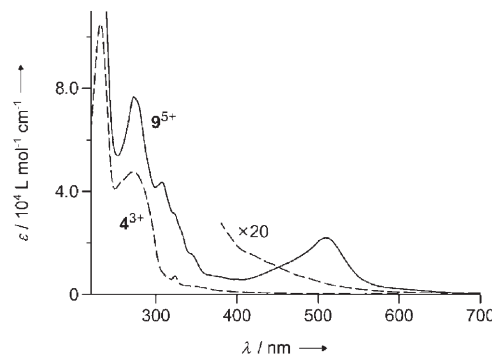


Figure 8. Absorption spectrum of the rotaxane ligand **4**³⁺ (dashed line) and complex **9**⁵⁺ (full line) in MeCN at room temperature.

arising from π -stacking between the electron-rich dioxyaromatic units of the macrocycles and the electron-poor pyridinium and 4,4'-bipyridinium units of the cationic axle.^[31]

In MeCN at room temperature the ligands 1^{3+} , 3^{3+} , and 4^{3+} exhibit the fluorescence band ($\lambda_{\max}=450$ nm) typical of 4'-methylpyridinium-2,2':6',2''-terpyridine (MePy-terpy). The intense fluorescence of DB24C8 ($\lambda_{\max}=305$ nm) and DN24C8 ($\lambda_{\max}=340$ nm; DN24C8=dinaphtho[24]crown-8 ether) is strongly quenched in 3^{3+} and 4^{3+} , respectively, presumably because the potentially fluorescent π - π^* singlet excited states of the dioxyaromatic units of the crown ethers undergo radiationless decay to the low-lying, nonemissive CT states.

Absorption and luminescence properties of the ruthenium(II) complexes: The absorption and luminescence data for the Ru^{II} complexes 6^{5+} - 9^{5+} are gathered in Table 2, together with those of the model compounds, $[\text{Ru}(\text{terpy})_2]^{2+}$ and $[\text{Ru}(\text{terpy})(\text{MePy-terpy})]^{3+}$.

First of all, it should be noted that compounds 6^{5+} - 9^{5+} are in fact complex multichromophoric systems that contain several different photoactive units capable of interacting with one another. For the sake of simplicity, we will denote these units as P, A, and R, that is, the photosensitizing Ru-based unit, the 4,4'-bipyridinium electron-accepting unit, and (in the case of 8^{5+} and 9^{5+}) the aromatic moieties of the crown ether rings, respectively.

The absorption spectra of ruthenium(II)-polypyridine complexes usually exhibit very intense bands in the UV region, generally assigned to ligand-centered (LC) π - π^* transitions, and moderately intense bands located in the visible region, resulting from spin allowed d_{π} - π^* metal-to-ligand charge-transfer (MLCT) transitions.^[23] The MLCT involves a metal-based HOMO and the ligand-based LUMO.^[32] In line with the above expectations, the absorption spectra of compounds 6^{5+} - 9^{5+} are dominated by the high energy π - π^* LC bands at around 270 and 305 nm and by the MLCT bands located at around 505 nm (see Figure 7 for 6^{5+} and Figure 8 for 9^{5+}). The MLCT bands, in the case of 8^{5+} and 9^{5+} , hide the weak absorption tail originating from the CT interactions between the electron-donor macrocycles and the 4,4'-bipyridinium unit [CT(R-A), vide supra]. The MLCT bands for these complexes are considerably red-

shifted with respect to that of the parent compound $[\text{Ru}(\text{terpy})_2]^{2+}$ (Table 2). This is most likely due to a stabilization of the π^* orbital caused by the electron-withdrawing nature of the methylpyridinium substituent on the terpy ligand. It was observed^[33] that the presence of electron-accepting or electron-donating substituents in the 4'-position of the terpy ligand affects the photophysical properties of the metal complex considerably. In fact, as it will be shown below, $[\text{Ru}(\text{terpy})_2]^{2+}$ is not a suitable model for the compounds examined here, and the heteroleptic complex $[\text{Ru}(\text{terpy})(\text{MePy-terpy})]^{3+}$ should be considered instead. The maximum of the MLCT band ranges from 504 nm in the absence of the crown ether (6^{4+}) to 510 nm for the DN24C8 based complex (9^{4+} ; Table 2). A slight stabilization of the singlet MLCT excited states relative to the ground state (red shift of the visible absorption band) is observed as the crown ether proceeds through the series DN24C8 > DB24C8 > 24C8 \approx no crown. A similar dependence was seen previously for a set of homoleptic iron(II) complexes with the same rotaxane ligands.^[19] At the present stage it is not clear whether such a stabilization effect is related to electronic or steric factors.

It can be noted that two weak absorption bands at very low energy are observed for the axle-like complex 6^{5+} (Table 2 and Figure 7). We tentatively assign these bands to CT transitions from a metal-centered d_{π} orbital to π^* orbitals localized on the 4,4'-bipyridinium unit [CT(P-A)].^[34] It seems unlikely that such a CT interaction be through bond because 1) the metal complex and 4,4'-bipyridinium moieties are electronically insulated by two methylene groups, and 2) the far red and infrared absorption bands are not observed for the rotaxane complexes. The inspection of physical CPK models suggests that folded conformations in which the A unit is close to the P unit can indeed exist for 6^{5+} , but not for the rotaxane complexes 7^{5+} - 9^{5+} , owing to the presence of the macrocycle, which enforces the *anti* conformation of the central NCH₂CH₂N ethane fragment. The energy of the lowest absorption band of 6^{5+} is consistent with the difference between the potential for the Ru^{III}-Ru^{II} process^[33] and that for the reduction of the 4,4'-bipyridinium unit,^[35] which can be taken as a measure of the energy difference between the two orbitals involved in the CT transition.

Table 2. Absorption and luminescence data.

Compound	Absorption ^[a]			Luminescence					
	298 K			298 K ^[a]			77 K ^[b]		
	λ_{\max} [nm]	ϵ [L mol ⁻¹ cm ⁻¹]		λ_{\max} [nm]	$I_{\text{rel}}^{\text{[c]}}$	τ [ns]	$k_{\text{q}}^{\text{[d]}}$	λ_{\max} [nm]	τ [μ s]
$[\text{Ru}(\text{terpy})_2]^{2+ \text{[c]}}$	270 (44 000)	308 (71 000)	474 (17 000)	629 ^[f]	< 0.01 ^[f]	0.25	–	598	11
$[\text{Ru}(\text{terpy})(\text{MePy-terpy})]^{3+ \text{[g]}}$	273 (54 000)	308 (45 000)	500 (23 000)	775	1 ^[h]	125	–	676	6.8
6^{5+} (no crown)	273 (55 000)	307 (39 000)	504 (14 000) 730 (780) 910 (480)	850	0.053	8.9	1.0×10^8	687	6.4
7^{5+} (24C8)	275 (70 000)	305 (42 000)	505 (21 000)	810	0.23	24	3.4×10^7	677	5.4
8^{5+} (DB24C8)	275 (74 000)	305 (43 000)	508 (23 000)	788	0.17	22	3.7×10^7	692	6.0
9^{5+} (DN24C8)	230 (153 000)	273 (77 000)	305 (43 000) 510 (22 000)	796	0.13	18	4.8×10^7	695	6.1

[a] Air equilibrated acetonitrile solution. [b] Butyronitrile rigid matrix. [c] Emission intensity relative to the $[\text{Ru}(\text{terpy})(\text{MePy-terpy})]^{3+}$ model compound. [d] Calculated by Equation (1) (see Experimental Section). [e] Data from reference [23]. [f] Data from reference [33]. [g] MePy-terpy = 4'-methylpyridinium-2,2':6',2''-terpyridine. [h] Conventionally taken as unit; the luminescence quantum yield of $[\text{Ru}(\text{terpy})(\text{MePy-terpy})]^{3+}$ was determined to be 3.0×10^{-4} .

Ru^{II}-polypyridine complexes typically show emission from their lowest energy ³MLCT level.^[23] However, [Ru(terpy)₂]²⁺ exhibits much less favorable photophysical properties (almost complete lack of luminescence and very short excited-state lifetime at room temperature) relative to, for example, [Ru(bpy)₃]²⁺. It is also known^[33] that the presence of electron-accepting substituents in the 4'-position of the terpy ligand causes a red shift of the emission band, and an increase of the luminescence quantum yield and the excited state lifetime at room temperature. By connecting a 1,2-bis-(pyridinium)ethane axle to one terpyridine ligand, we could make Ru-based metal complexes with a strongly electron-accepting pyridinium moiety linked directly to the 4'-position of terpy that should exhibit room-temperature luminescence. This expectation is fully confirmed by comparing the luminescence properties of [Ru(terpy)(MePy-terpy)]³⁺ and [Ru(terpy)₂]²⁺ (Table 2). Clearly, [Ru(terpy)(MePy-terpy)]³⁺, unlike [Ru(terpy)₂]²⁺, is a suitable model for the metal complex moiety of the compounds examined here. The MLCT luminescence band typical of the P unit, observed in MeCN at room temperature for complexes **6**⁵⁺–**9**⁵⁺, is shifted to lower energies relative to the [Ru(terpy)(MePy-terpy)]³⁺ model complex (Table 2 and Figure 9), suggesting that the A

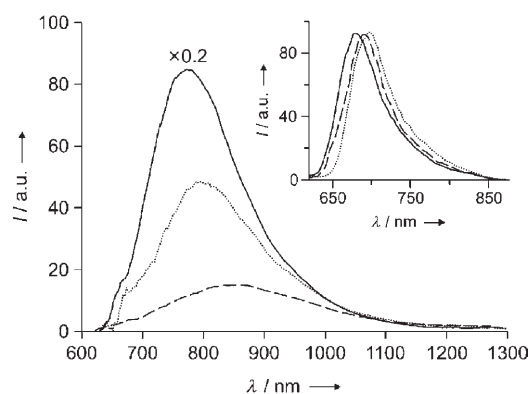


Figure 9. Corrected luminescence spectra of [Ru(terpy)(MePy-terpy)]³⁺ (full line), **6**⁵⁺ (dashed line), and **9**⁵⁺ (dotted line) in MeCN at room temperature and (inset) in butyronitrile rigid matrix at 77 K. Excitation was performed in the maximum of the MLCT absorption band. The emission bands obtained at 77 K are normalized at the maximum intensity.

unit of the axle provides a stabilization of the π^* orbital of the MePy-terpy ligand. The maximum of the MLCT luminescence band, however, does not show a clear dependence on the type of crown ether surrounding the cationic axle. The lowest energy luminescence among the examined compounds is exhibited by the axle complex **6**⁵⁺. A contribution from low-energy emission transitions originated by the CT(P–A) states can be ruled out, because we could not see any luminescence band in the near infrared upon excitation of **6**⁵⁺ at $\lambda > 700$ nm.

The room-temperature luminescence of compounds **6**⁵⁺–**9**⁵⁺ is considerably quenched relative to that of the [Ru(terpy)(MePy-terpy)]³⁺ model. The values of the rate constants for the quenching process, evaluated from the lumi-

nescence lifetime measurements (Table 2), are much smaller than those observed for related Ru-based complexes bearing a covalently linked 4,4'-bipyridinium unit.^[12,36] Nevertheless, the efficiency of the quenching process in these compounds is high (from 81% for **8**⁵⁺ to 90% for **6**⁵⁺). The luminescence quenching is interpreted in terms of an electron transfer from the ³MLCT excited state of the Ru-based unit to the 4,4'-bipyridinium unit, as found for the previously investigated systems.^[12,36] Interestingly, when a crown ether surrounds the cationic axle as in **7**⁵⁺–**9**⁵⁺, the photoinduced electron-transfer process is slowed down by a factor from 2 to 3 with respect to the ringless compound **6**⁵⁺ (Table 2). We attribute such an effect to the presence of the macrocycle in the rotaxane complexes, which prevents the formation of folded structures characterized by a fast electron-transfer process.

In butyronitrile rigid matrix at 77 K, the luminescence lifetime of the Ru-based unit of compounds **6**⁵⁺–**9**⁵⁺ is not quenched at all (Table 2). In fact, under these conditions the electron-transfer quenching process is most likely endergonic, because of the lack of solvent repolarization.^[37] In principle, for **6**⁵⁺ energy transfer from the ³MLCT states to the lower lying CT(P–A) states involving the 4,4'-bipyridinium unit could also occur. This possibility is difficult to investigate, because such CT states are not emissive (vide supra). However, the fact that the luminescence of **6**⁵⁺ at 77 K is not quenched suggests that either in a rigid medium the CT(P–A) states are much more destabilized relative to the ³MLCT levels, or the folded conformations do not contribute appreciably to the overall population of the **6**⁵⁺ species.

In all cases the excitation spectra recorded in the UV region for the Ru-based emission indicate that the electronic energy transfer from the 4,4'-bipyridinium unit to the metal complex moiety is not complete; however, the efficiency of the process is difficult to evaluate, because intense LC bands of the Ru-based component overlap with the absorption band of the 4,4'-bipyridinium unit (Figures 7 and 8).

The photoinduced processes taking place in the examined complexes can be summarized with the generalized energy level diagram shown in Figure 10. The energy values for the ³MLCT and S₁ levels have been obtained from the highest energy feature of the emission spectra at 77 K; as a rough estimation of the energy of ¹MLCT, CT(P–A), and CT(R–A) levels we have taken the maximum of the corresponding absorption bands. The energy of the P⁺–A[–] state is assumed to be that determined from the reduction potentials of [Ru(terpy)₂]³⁺ (+1.30 V vs. SCE)^[23] and 1,1'-dibenzyl-4,4'-bipyridinium (–0.35 V vs. SCE).^[35] At room temperature, excitation of the Ru-based unit (P) with visible light leads to the formation of its ³MLCT level (via the ¹MLCT state), followed by an electron transfer to the 4,4'-bipyridinium unit (A) to give the P⁺–A[–] species. In rigid matrix at 77 K, the luminescence of the P unit is not affected by the presence of the A moiety, because the electron-transfer quenching process cannot occur under such conditions due to destabilization of the P⁺–A[–] species. UV excitation of the aromatic units of the macrocycle R in the case of **8**⁵⁺ and **9**⁵⁺ causes

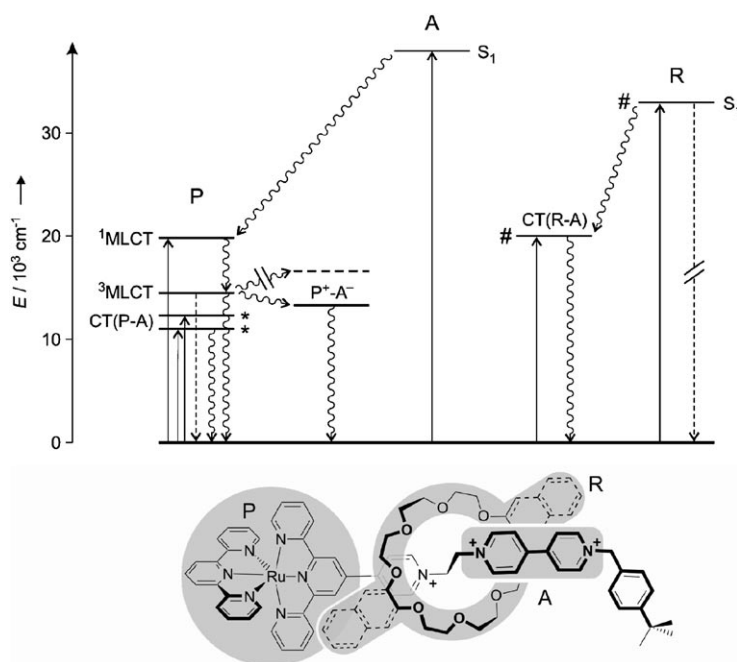


Figure 10. Generalized energy level diagram for complexes 6^{5+} – 9^{5+} in a simplified representation in which the Ru-based photosensitizing unit, the 4,4'-bipyridinium electron accepting unit and the macrocyclic ring are denoted as P, A, and R, respectively. The levels marked with * are observed only for axle-like complex 6^{5+} , whereas the levels marked with # are observed only for rotaxane complexes 8^{5+} and 9^{5+} . The observed absorption (full lines), emission (dashed lines) and radiationless (wavy lines) processes are indicated. The horizontal dotted line represents an estimation of the P^+-A^- energy level in rigid matrix at 77 K. For more details, see the text.

the population of their potentially fluorescent S_1 levels, which are strongly quenched, most likely by the lower lying CT(R–A) states originating from electron-donor–acceptor interactions with the A unit. Compound 6^{5+} shows also the presence of energy levels assigned to charge transfer from a metal-centered d_{π} orbital to π^* orbitals localized on the A unit [CT(P–A)].

Conclusion

We have synthesized a series of heteroleptic Ru^{II} complexes in which one of the two terpy ligands is covalently linked to a [2]rotaxane moiety based on the 1,2-bis(pyridinium)ethane- \subset [24]crown-8 ether motif. The characterization of the compounds by 1D and 2D ¹H NMR spectroscopy, X-ray crystallography, high-resolution electrospray ionization mass spectrometry, and UV/visible/NIR absorption and emission spectroscopy has evidenced a wealth of intercomponent interactions. Unlike parent [Ru(terpy)₂]²⁺, the examined complexes exhibit a luminescence band in the near infrared spectral region and a relatively long lifetime of the ³MLCT excited state. Visible excitation of the Ru-based chromophore in MeCN at room temperature causes an efficient electron transfer to the covalently linked 4,4'-bipyridinium unit of the axle. Such a process is slowed down by a factor of 2 to 3 when a crown ether surrounds the cationic axle, and it is totally blocked in rigid matrix at 77 K. These favor-

able photophysical properties, together with the structural advantages offered by Ru^{II}-bis-(terdentate) complexes, make the present compounds interesting candidates for the construction of photochemical devices with a linear geometry. The possibility of conformational rearrangements of the rotaxanes upon light excitation is currently under investigation.

Experimental Section

General methods: 2,2':6',2''-Terpyridine was obtained from Aldrich and used as received. RuCl₃·xH₂O and [Ru(bpy)₃][Cl]₂ were obtained from Strem and used as received. [RuCl₃(terpy)],^[38] [Ru(terterpy)₂][OTf]₂,^[39] [Ru(terpy)₂][OTf]₂^[39] and [Mepy-terpy]^[40] were synthesized using literature methods. Compounds **1–4**[OTf]₃ were synthesized as previously reported.^[19] Solvents were dried by using Innovative Technologies Solvent Purification Systems. Thin-layer chromatography (TLC) were performed on Merck Silica gel 60 F₂₅₄ plates and viewed under UV light. Column chromatography was performed by using Silicycle Ultra Pure Silica Gel (230–400 mesh). ¹H NMR spectra were obtained on a Bruker Avance 500 instrument operating at 500.1 MHz (with the deuterated solvent as the lock and the residual solvent or tetramethylsilane as the internal reference). Both 1D ¹H NMR and conventional 2D NMR (¹H–¹H COSY, ¹H–¹H LRCOSY and ¹H–¹H NOESY) spectroscopic measurements were used to assign all peaks. Deuterated solvents were purchased from Cambridge Isotope Laboratories and used as received. High-resolution mass spectra were recorded in MeCN/H₂O (50:50) on a Micromass LCT Electrospray TOF mass spectrometer.

Synthesis of the ruthenium(II) complexes: Model complex [Ru(terpy)(Mepy-terpy)][OTf]₃ and the Ru–terpy based rotaxanes 6^{5+} – 9^{5+} were prepared by using the appropriate pyridinium ligand ([Mepy-terpy]-[OTf] or **1–4**[OTf]₃) as described in detail here for **8**[OTf]₃. Solid [RuCl₃(terpy)] (0.012 g, 0.027 mmol) was added to a solution of **1**³⁺ (0.043 g, 0.027 mmol) dissolved in EtOH/H₂O (1:1) and the mixture was brought to reflux for 24 h to give a deep red solution. The reaction mixture was cooled to room temperature and filtered through a Celite pad washing with EtOH until the eluent was colourless. The filtrate was then reduced to half the volume and the addition of NaOTf produced a red precipitate. The red solid was purified by column chromatography (MeOH/2 M NH₄Cl/MeNO₂ 3:1:1). The fractions containing the product were evaporated under reduced pressure and redissolved in H₂O. Following salt metathesis with NaOTf and collection by vacuum filtration the compound, **8**[OTf]₃, was isolated as a red solid (0.017 g, 29%). ¹H NMR (500 MHz, [D₃]MeCN, 25 °C): δ = 9.39 (m, 2H; H_g), 9.39 (m, 2H; H_i), 8.98 (m, 2H; H_m), 8.96 (s, 2H; H_e), 8.84 (d, ³J_{d,c} = 8.1 Hz, 2H; H_d), 8.81 (d, ³J_{e,f} = 8.2 Hz, 2H; H_e), 8.74 (d, ³J_{f,g} = 6.7 Hz, 2H; H_f), 8.54 (d, ³J_{d,c'} = 8.1 Hz, 2H; H_{d'}), 8.49 (t, ³J_{f,e'} = 8.2 Hz, 1H; H_{f'}), 8.20 (d, ³J_{j,k} = 6.8 Hz, 2H; H_j), 8.14 (d, ³J_{l,m} = 6.8 Hz, 2H; H_l), 8.05 (ddd, ³J_{c,b} ≈ ³J_{c,d} = 6.6 Hz, ⁴J_{c,a} = 1.1 Hz, 2H; H_c), 7.97 (ddd, ³J_{e,b'} ≈ ³J_{e,d'} = 7.6 Hz, ⁴J_{e,a'} = 1.4 Hz, 2H; H_e), 7.60 (d, ³J_{p,o} = 8.4 Hz, 2H; H_p), 7.49 (d, ³J_{o,p} = 8.4 Hz, 2H; H_o), 7.44 (d,

$^3J_{a,b} = 5.7$ Hz, 2H; H_a), 7.35 (d, $^3J_{a,b'} = 4.8$ Hz, 2H; H_a'), 7.28 (ddd, $^3J_{b,a} \approx ^3J_{b,c} = 7.0$ Hz, $^4J_{b,d} \approx 1.0$ Hz, 2H; H_b), 7.22 (ddd, $^3J_{b',a'} \approx ^3J_{b',c'} = 6.2$ Hz, $^4J_{b',d'} \approx 0.8$ Hz, 2H; $H_{b'}$), 6.77 (m, 4H; H_i), 6.50 (m, 4H; $H_{i'}$), 5.82 (s, 2H; H_m), 5.70 (m, 2H; H_h), 5.70 (m, 2H; H_i), 4.18–4.01 (m, 24H; H_v , H_w , H_x), 1.34 ppm (s, 9H; H_q); HR ESI-MS: m/z calcd for $C_{86}H_{84}N_9O_{20}F_{12}S_4Ru [M-OTf]^+$: 2020.3567; found: 2020.3636.

[Ru(terpy)(Mepy-terpy)](OTf)₃: Yield: 78%; 1H NMR (500 MHz, [D₃]MeCN, 25 °C): $\delta = 9.19$ (s, 2H; H_e), 8.96 (d, $^3J_{d,c} = 7.0$ Hz, 2H; H_d), 8.81 (m, 2H; H_g), 8.79 (d, $^3J_{e,f} = 8.1$ Hz, 2H; H_e), 8.74 (d, $^3J_{f,g} = 7.0$ Hz, 2H; H_f), 8.51 (d, $^3J_{d,c'} = 7.0$ Hz, 2H; H_d'), 8.46 (t, $^3J_{f,e'} = 8.1$ Hz, 2H; H_f'), 7.98 (ddd, $^3J_{c,b} \approx ^3J_{c,d} = 7.8$ Hz, $^4J_{c,a} = 1.2$ Hz, 2H; H_c), 7.92 (ddd, $^3J_{c',b'} \approx ^3J_{c',d'} = 8.0$ Hz, $^4J_{c',a'} = 1.3$ Hz, 2H; H_c'), 7.39 (m, 2H; H_a), 7.39 (m, 2H; H_a'), 7.24 (ddd, $^3J_{b,c} \approx ^3J_{b,a} = 5.6$ Hz, $^4J_{d,b} = 1.1$ Hz, 2H; H_b), 7.16 (ddd, $^3J_{b',a'} \approx ^3J_{b',c'} = 5.7$ Hz, $^4J_{b',d'} = 1.1$ Hz, 2H; $H_{b'}$), 4.46 ppm (s, 3H; H_h); HR ESI-MS: m/z calcd for $C_{39}H_{38}N_7O_9F_9S_3Ru [M-OTf]^+$: 1107.0010; found: 1107.0008.

Compound 6(OTf)₃: Column chromatography carried out on silica by using MeCN/H₂O/satd KNO₃ (5:4:1) as the eluent. Yield: 43%; 1H NMR (500 MHz, [D₃]MeCN, 25 °C): $\delta = 9.25$ (s, 2H; H_e), 9.11 (m, 2H; H_g), 9.11 (m, 2H; H_i), 9.02 (d, $^3J_{m,l} = 6.9$ Hz, 2H; H_m), 8.94 (d, $^3J_{d,c} = 7.0$ Hz, 2H; H_d), 8.79 (d, $^3J_{e,f} = 8.1$ Hz, 2H; H_e), 8.75 (d, $^3J_{f,g} = 7.0$ Hz, 2H; H_f), 8.56 (d, $^3J_{d,c'} = 7.0$ Hz, 2H; H_d'), 8.50 (m, 2H; H_k), 8.50 (m, 2H; H_i), 8.46 (t, $^3J_{f,e'} = 8.1$ Hz, 2H; H_f'), 7.97 (ddd, $^3J_{c,b} \approx ^3J_{c,d} = 7.8$ Hz, $^4J_{c,a} = 1.2$ Hz, 2H; H_c), 7.92 (ddd, $^3J_{c',b'} \approx ^3J_{c',d'} = 8.0$ Hz, $^4J_{c',a'} = 1.3$ Hz, 2H; H_c'), 7.54 (d, $^3J_{p,o} = 8.4$ Hz, 2H; H_p), 7.45 (d, $^3J_{o,p} = 8.4$ Hz, 2H; H_o), 7.39 (m, 2H; H_a), 7.39 (m, 2H; H_a'), 7.21 (ddd, $^3J_{b,c} \approx ^3J_{b,a} = 5.6$ Hz, $^4J_{d,b} = 1.1$ Hz, 2H; H_b), 7.15 (ddd, $^3J_{b',a'} \approx ^3J_{b',c'} = 5.7$ Hz, $^4J_{b',d'} = 1.1$ Hz, 2H; $H_{b'}$), 5.80 (s, 2H; H_n), 5.38 (m, 2H; H_h), 5.38 (m, 2H; H_i), 1.37 ppm (s, 9H; H_q); HR ESI-MS: m/z calcd for $C_{62}H_{52}N_9O_{12}F_{12}S_4Ru [M-OTf]^+$: 1572.1470; found: 1572.1466.

Compound 7(OTf)₃: Yield: 24%; 1H NMR (500 MHz, [D₃]MeCN, 25 °C): $\delta = 9.40$ (m, 2H; H_g), 9.40 (m, 2H; H_i), 9.34 (s, 2H; H_e), 9.08 (m, 2H; H_j), 9.08 (m, 2H; H_m), 8.87 (d, $^3J_{d,c} = 8.0$ Hz, 2H; H_d), 8.80 (d, $^3J_{e,f} = 8.2$ Hz, 2H; H_e), 8.61 (d, $^3J_{k,j} = 6.7$ Hz, 2H; H_k), 8.53 (m, 2H; H_j), 8.53 (m, 2H; H_d'), 8.47 (t, $^3J_{f,e'} = 8.2$ Hz, 2H; H_f'), 7.99 (ddd, $^3J_{c,b} \approx ^3J_{c,d} = 7.7$ Hz, $^4J_{c,a} = 1.2$ Hz, 2H; H_c), 7.93 (ddd, $^3J_{c',b'} \approx ^3J_{c',d'} = 7.0$ Hz, $^4J_{c',a'} = 1.2$ Hz, 2H; H_c'), 7.57 (d, $^3J_{p,o} = 8.3$ Hz, 2H; H_p), 7.49 (d, $^3J_{o,p} = 8.3$ Hz, 2H; H_o), 7.42 (m, 2H; H_a), 7.42 (m, 2H; H_a'), 7.24 (ddd, $^3J_{b,c} \approx ^3J_{b,a} = 6.4$ Hz, $^4J_{d,b} = 1.1$ Hz, 2H; H_b), 7.18 (ddd, $^3J_{b',a'} \approx ^3J_{b',c'} = 7.0$ Hz, $^4J_{b',d'} = 1.0$ Hz, 2H; $H_{b'}$), 5.84 (s, 2H; H_n), 5.53 (m, 2H; H_h), 5.53 (m, 2H; H_i), 3.60 (m, 32H; H_v), 1.33 ppm (m, 9H; H_q); HR ESI-MS: m/z calcd for $C_{77}H_{84}N_9O_{17}F_9S_3Ru [M-2OTf]^+$: 887.7034; found: 887.7032.

Compound 9(OTf)₃: Yield: 22%; 1H NMR (500 MHz, [D₃]MeCN, 25 °C): $\delta = 9.42$ (m, 2H; H_g), 9.42 (m, 2H; H_i), 8.80 (d, $^3J_{e,f} = 8.2$ Hz, 2H; H_e), 8.70 (d, $^3J_{m,l} = 6.7$ Hz, 2H; H_m), 8.59 (m, 2H; H_j), 8.59 (m, 2H; H_d'), 8.54 (d, $^3J_{d,c} = 8.0$ Hz, 2H; H_d), 8.51 (s, 2H; H_e), 8.47 (t, $^3J_{f,e'} = 8.2$ Hz, 2H; H_f'), 8.23 (d, $^3J_{k,j} = 6.7$ Hz, 2H; H_k), 7.99 (ddd, $^3J_{c,b} \approx ^3J_{c,d} = 8.0$ Hz, $^4J_{c,a} = 1.5$ Hz, 2H; H_c), 7.97 (ddd, $^3J_{c',b'} \approx ^3J_{c',d'} = 8.0$ Hz, $^4J_{c',a'} = 1.5$ Hz, 2H; H_c'), 7.70 (d, $^3J_{p,o} = 6.7$ Hz, 2H; H_p), 7.66 (d, $^3J_{o,p} = 8.4$ Hz, 2H; H_o), 7.51 (d, $^3J_{o,p} = 8.4$ Hz, 2H; H_o), 7.43 (m, 4H; H_i), 7.37 (d, $^3J_{a,b'} = 5.0$ Hz, 2H; H_a'), 7.28 (ddd, $^3J_{b,c} \approx ^3J_{b,a} = 7.3$ Hz, $^4J_{d,b} = 1.1$ Hz, 2H; H_b), 7.24 (m, 2H; H_a), 7.24 (m, 2H; H_b), 7.12 (s, 4H; H_n), 6.65 (m, 4H; H_i), 5.75 (m, 2H; H_h), 5.75 (m, 2H; H_j), 5.66 (s, 2H; H_n), 4.29–4.16 ppm (m, 24H; H_v , H_w , H_x), 1.36 (m, 9H; H_q); HR ESI-MS: m/z calcd for $C_{94}H_{88}N_9O_{20}F_{12}S_4Ru [M-OTf]^+$: 2120.3880; found: 2120.3975.

X-ray diffraction studies: Single crystals of **8(OTf)₃** suitable for X-ray analysis were grown by slow diffusion of isopropylether into a solution of the compound and a small amount of NET₄Cl in MeCN. Crystals could only be grown in the presence of a chloride ion, which was incorporated in a nonstoichiometric manner into the structure as a non-coordinating anion. Although the data was not of particularly good quality, a satisfactory structural solution was possible with some restraints as outlined. Single crystals of **9(OTf)₃** suitable for x-ray analysis were grown by slow diffusion of isopropylether into a solution of the compound in MeCN.

Both crystals were mounted in a cryoloop with paratone oil. Data were collected on a Bruker APEX CCD single-crystal diffractometer with MoK α radiation ($\lambda = 0.71073$ Å). Reflection data were integrated from frame data obtained from hemisphere scans. Decay (<1%) was monitored by 50 standard data frames measured at the beginning and end of

data collection. Diffraction data and unit-cell parameters were consistent with assigned space groups. Lorentzian polarization corrections and empirical absorption corrections, based on redundant data at varying effective azimuthal angles, were applied to both data sets. The structures were solved by direct methods, completed by subsequent Fourier syntheses and refined with full-matrix least-squares methods against $|F^2|$ data. All non-hydrogen atoms were refined anisotropically. All hydrogen atoms not involved in hydrogen bonding were treated as idealized contributions. All hydrogen atoms involved in hydrogen bonding were refined isotropically. Scattering factors and anomalous dispersion coefficients were contained in the SHELXTL 5.03 program library.^[41] Structure drawings were generated by using the program DIAMOND 3.1.^[42] CCDC-286045 (**8(OTf)₃**) and CCDC-286046 (**9(OTf)₃**) contain the supplementary crystallographic data for this paper. These data can be obtained free of charge from the Cambridge Crystallographic Data Center via www.ccdc.cam.ac.uk/data_request/cif.

Crystal data for 8(OTf)₃: $C_{86.50}Cl_{0.25}F_{13.50}N_9O_{26.50}RuS_5$, $M_r = 2200.36$, triclinic, space group $P\bar{1}$, $a = 21.0193(15)$, $b = 24.5878(17)$, $c = 26.3294(18)$ Å, $\alpha = 103.899(2)^\circ$, $\beta = 104.742(2)^\circ$, $\gamma = 111.360(2)^\circ$, $V = 11387.8(14)$ Å³, $T = 173(2)$ K, $Z = 4$, $\mu = 0.325$ mm⁻¹, 61 087 independent reflections ($R_{int} = 0.0857$); $R1 = 0.1505$, $wR2 = 0.3861$ [$I > 2\sigma(I)$]; $R1 = 0.2085$, $wR2 = 0.4149$ (all data); goodness-of-fit (F^2) = 1.340.

Crystal data for 9(OTf)₃: $C_{95}H_{88}F_{15}N_9O_{33}RuS_5$, $M_r = 2430.11$, monoclinic, space group $P2_1/c$, $a = 24.0869(13)$, $b = 20.0588(11)$, $c = 22.4599(12)$ Å, $\beta = 91.909(1)^\circ$, $V = 10845.6(10)$ Å³, $T = 173(2)$ K, $Z = 4$, $\mu = 0.349$ mm⁻¹, 19 091 independent reflections ($R_{int} = 0.0649$); $R1 = 0.0884$, $wR2 = 0.2374$, [$I > 2\sigma(I)$]; $R1 = 0.1187$, $wR2 = 0.2628$ (all data); goodness-of-fit (F^2) = 1.060.

Absorption and emission spectra: The measurements were carried out at room temperature in air-equilibrated solutions of the samples in MeCN (Merck Uvasol[®]) at a concentration ranging from 5×10^{-6} to 1×10^{-4} mol L⁻¹ and contained in quartz cells with 1.0 cm path length. Luminescence spectra at 77 K were recorded on a butyronitrile (Fluka) rigid matrix contained in a glass tube immersed in a glass dewar filled with liquid nitrogen. UV/Vis/NIR absorption spectra were recorded with a Perkin–Elmer Lambda 40 spectrophotometer, whereas UV/Vis luminescence spectra were recorded with a Perkin–Elmer LS-50 spectrofluorimeter. The luminescence spectra in the far red and near IR spectral regions were obtained with an Edinburgh FLS920 spectrometer equipped with a Hamamatsu R5509–72 supercooled photomultiplier tube (193 K) and a TM300 emission monochromator with NIR grating blazed at 1000 nm; a 450 W xenon arc lamp was used as light source. In all cases the emission spectra were corrected to compensate for the photomultiplier response in the different spectral regions. When necessary, luminescence data were also corrected for the luminescence intensity versus absorbance instrumental response and inner filter effects.^[43,44] Emission quantum yields were measured at room temperature in air-equilibrated solutions by using [Os(bpy)₃][PF₆]₂ in deoxygenated MeCN ($\phi = 0.005$) as reference compound.^[44,45] Luminescence lifetime measurements were obtained by using an Edinburgh Analytical Instruments (EAI) time-correlated single-photon counting apparatus, equipped with a cooled (ca. –20 °C) Hamamatsu R928-P photomultiplier tube; the excitation pulse was obtained by a pulsed diode laser (406 nm Picoquant). Data correlation and manipulation were carried out using EAI F900 software version 6.35. Emission lifetimes were calculated using a single-exponential fitting function; a Levenberg–Marquardt algorithm with iterative reconvolution Edinburgh instruments F900 software was used. The reduced χ^2 and residual plots were used to judge the quality of the fits. Band maxima, relative luminescence intensities, and luminescence lifetimes were measured with estimated uncertainties of 2 nm, 20%, and 10%, respectively. The rate constants of the intercomponent electron-transfer quenching processes were evaluated by the use of Equations (1) and (2).

$$k_q = \frac{1}{\tau} - \frac{1}{\tau_0} \quad (1)$$

$$k_q = \frac{1}{\tau_0} \left(\frac{I_0}{I} - 1 \right) \quad (2)$$

In Equations (1) and (2) I_0 and τ_0 are the luminescence intensity and lifetime of the reference compound [Ru(terpy)(MePy-terpy)]³⁺, respectively, and I and τ are the luminescence intensity and lifetime, respectively, of the examined compound under the same experimental and instrumental conditions.

Acknowledgements

We thank the Natural Sciences and Engineering Council of Canada, the European Union (STREP "Biomach" NMP4-CT-2003-505487), and the Italian MIUR (PRIN "Supramolecular Devices" and FIRB RBNE019H9K) for financial support of this research. G.J.E.D. is grateful for the award of an Ontario Graduate Scholarship.

- [1] V. Balzani, A. Credi, M. Venturi, *Molecular Devices and Machines—A Journey into the Nano World*, Wiley-VCH, Weinheim, 2003.
- [2] *Top. Curr. Chem.* **2005**, 262 (Special Volume on Molecular Motors; Guest Editor: T. R. Kelly).
- [3] D. B. Amabilino, J. F. Stoddart, *Chem. Rev.* **1995**, 95, 2725.
- [4] J. F. Stoddart, *Acc. Chem. Res.* **2001**, 34, 410.
- [5] A. N. Shipway, I. Willner, *Acc. Chem. Res.* **2001**, 34, 421.
- [6] A. R. Pease, J. O. Jeppesen, J. F. Stoddart, Y. Luo, C. P. Collier, J. R. Heath, *Acc. Chem. Res.* **2001**, 34, 433.
- [7] R. Ballardini, V. Balzani, A. Credi, M. T. Gandolfi, M. Venturi, *Acc. Chem. Res.* **2001**, 34, 445.
- [8] A. Harada, *Acc. Chem. Res.* **2001**, 34, 456.
- [9] C. A. Schalley, K. Beizai, F. Vögtle, *Acc. Chem. Res.* **2001**, 34, 465.
- [10] J. V. Hernández, E. R. Kay, D. A. Leigh, *Science* **2004**, 306, 1532.
- [11] J.-P. Sauvage, *Chem. Commun.* **2005**, 1507.
- [12] For examples of metal complexes with threaded or interlocked compounds as ligands, see reference [11] and: a) P. R. Ashton, V. Balzani, A. Credi, O. Kocian, D. Pasini, L. Prodi, N. Spencer, J. F. Stoddart, M. S. Tolley, M. Venturi, A. J. P. White, D. J. Williams, *Chem. Eur. J.* **1998**, 4, 590; b) P. R. Mackie, A. Harriman, *Angew. Chem.* **1998**, 110, 376; *Angew. Chem. Int. Ed.* **1998**, 37, 354; c) P. R. Ashton, R. Ballardini, V. Balzani, E. C. Constable, A. Credi, O. Kocian, S. J. Langford, J. A. Preece, L. Prodi, E. R. Schofield, N. Spencer, J. F. Stoddart, S. Wenger, *Chem. Eur. J.* **1998**, 4, 2413; d) P. R. Ashton, R. Ballardini, V. Balzani, A. Credi, R. Dress, E. Ishow, C. J. Kleverlaan, O. Kocian, J. A. Preece, N. Spencer, J. F. Stoddart, M. Venturi, S. Wenger, *Chem. Eur. J.* **2000**, 6, 3558.
- [13] S. J. Loeb, J. A. Wisner, *Angew. Chem.* **1998**, 110, 3010; *Angew. Chem. Int. Ed.* **1998**, 37, 2838.
- [14] S. J. Loeb, J. A. Wisner, *Chem. Commun.* **1998**, 2757.
- [15] S. J. Loeb, J. A. Wisner, *Chem. Commun.* **2000**, 845.
- [16] S. J. Loeb, J. A. Wisner, *Chem. Commun.* **2000**, 1939.
- [17] L. Hubbard, G. J. E. Davidson, R. H. Patel, J. A. Wisner, S. J. Loeb, *Chem. Commun.* **2004**, 138.
- [18] S. J. Loeb, *Chem. Commun.* **2005**, 1511.
- [19] G. J. E. Davidson, S. J. Loeb, *Dalton Trans.* **2003**, 23, 4319; for a recent review of supramolecular chemistry using terpyridines see: H. Hofmeier, U. S. Schubert, *Chem. Soc. Rev.* **2004**, 33, 373.
- [20] Utilizing various counterions, we have recorded ¹H NMR spectra of these [2]rotaxane ligands in deuterated CH₂Cl₂, CHCl₃, acetone, MeCN, MeNO₂, MeOH, DMF, DMSO, and water. In all cases, the [2]rotaxanes remained intact with no evidence of unthreading or decomposition.
- [21] V. Balzani, F. Scandola, *Supramolecular Photochemistry*, Horwood, Chichester, **1991**.
- [22] A. Juris, V. Balzani, F. Barigelli, S. Campagna, P. Belser, A. von Zelewsky, *Coord. Chem. Rev.* **1988**, 84, 85.
- [23] J.-P. Sauvage, J.-P. Collin, J.-C. Chambron, S. Guillerez, C. Coudret, V. Balzani, F. Barigelli, L. De Cola, L. Flamigni, *Chem. Rev.* **1994**, 94, 993.
- [24] a) J.-P. Collin, S. Guillerez, J.-P. Sauvage, *J. Chem. Soc. Chem. Commun.* **1989**, 776; b) J.-P. Collin, S. Guillerez, J.-P. Sauvage, F. Barigelli, L. De Cola, L. Flamigni, V. Balzani, *Inorg. Chem.* **1991**, 30, 4230.
- [25] a) E. C. Constable, A. M. W. Cargill Thomson, *J. Chem. Soc. Dalton Trans.* **1992**, 3467; b) E. C. Constable, in *Transition Metals in Supramolecular Chemistry* (Eds.: L. Fabbri, A. Poggi), Kluwer, Dordrecht, **1994**, p. 81.
- [26] Recent examples: a) E. Baranoff, J.-P. Collin, L. Flamigni, J.-P. Sauvage, *Chem. Soc. Rev.* **2004**, 33, 147, and references therein; b) E. C. Constable, R. W. Handel, C. E. Housecroft, A. F. Morales, B. Ventura, L. Flamigni, F. Barigelli, *Chem. Eur. J.* **2005**, 11, 4024.
- [27] C. A. Hunter, J. K. M. Sanders, *J. Am. Chem. Soc.* **1990**, 112, 5525.
- [28] B. N. Figgis, E. S. Kucharski, A. H. White, *Aust. J. Chem.* **1983**, 36, 1563.
- [29] E. C. Constable, A. M. W. Cargill Thompson, *New J. Chem.* **1992**, 16, 855.
- [30] Ligand 2³⁺ was not investigated fully. After repeated attempts to purify this material by chromatography, a quantity of sample of sufficient purity for spectroscopic measurements could not be obtained. Fortunately, pure samples of the Ru complex 7⁶⁺ could be prepared using 2³⁺ of ~95% purity.
- [31] P. R. Ashton, R.; Ballardini, V. Balzani, M. C. T. Fyfe, M. T. Gandolfi, M. V. Martínez-Díaz, M. Morosini, C. Schiavo, K. Shibata, J. F. Stoddart, A. J. P. White, D. J. Williams, *Chem. Eur. J.* **1998**, 4, 2332.
- [32] V. Balzani, A. Juris, M. Venturi, S. Campagna, S. Serroni, *Chem. Rev.* **1996**, 96, 759.
- [33] M. Maestri, N. Armaroli, V. Balzani, E. C. Constable, A. M. W. Cargill Thompson, *Inorg. Chem.* **1995**, 34, 2759.
- [34] B. P. Sullivan, H. Abruna, H. O. Finklea, D. J. Salmon, J. K. Nagle, T. J. Meyer, H. Sprintschnik, *Chem. Phys. Lett.* **1978**, 58, 389.
- [35] P. M. S. Monk, *The Viologens. Physicochemical Properties, Synthesis and Application of the Salts of 4,4'-Bipyridine*, Wiley, Chichester, **1998**.
- [36] a) E. H. Yonemoto, R. L. Riley, Y. L. Kim, S. J. Atherton, R. H. Schmehl, T. E. Mallouk, *J. Am. Chem. Soc.* **1992**, 114, 8081; b) E. H. Yonemoto, G. B. Saube, R. H. Schmehl, S. M. Hubig, R. L. Riley, B. L. Iverson, T. E. Mallouk, *J. Am. Chem. Soc.* **1994**, 116, 4786; c) L. A. Kelly, M. A. J. Rodgers, *J. Phys. Chem.* **1995**, 99, 13132.
- [37] a) M. R. Wasielewski, D. G. Johnson, W. A. Svec, K. M. Kersey, D. W. Minsek, *J. Am. Chem. Soc.* **1988**, 110, 7219; b) P. Chen, T. J. Meyer, *Inorg. Chem.* **1996**, 35, 5520.
- [38] A. P. Sullivan, J. M. Calvert, T. J. Meyer, *Inorg. Chem.* **1980**, 19, 1404.
- [39] R. P. Thummel, V. Hedge, Y. Jahng, *Inorg. Chem.* **1989**, 28, 3264.
- [40] L. Persaud, G. Barbiero, *Can. J. Chem.* **1991**, 69, 315.
- [41] G. M. Sheldrick, SHELXTL 5.03 Program Library, Brüker Analytical Instrument Division, Madison, Wisconsin, USA, **1997**.
- [42] DIAMOND-Visual Crystal Structure Information System, Version 3.1. Crystal Impact, Postfach 1251, 53002 Bonn, Germany.
- [43] A. Credi, L. Prodi, *Spectrochim. Acta Part A* **1998**, 54, 159.
- [44] *Handbook of Photochemistry*, 3rd ed. (Eds.: M. Montalti, A. Credi, L. Prodi, M. T. Gandolfi), CRC, Boca Raton, in press; section 10.
- [45] E. M. Kober, J. V. Caspar, R. S. Lumpkin, T. J. Meyer, *J. Phys. Chem.* **1986**, 90, 3722.

Received: October 7, 2005
Published online: February 7, 2006